A&A manuscript no.
(will be inserted by hand later)

Your thesaurus codes are:
07(02.08.1;02.18.7;08.03.1;08.03.4;08.12.1)

ASTRONOMY
AND
ASTROPHYSICS
18.5.1994

Circumstellar Dust Shells around Long-period Variables

II. Theoretical lightcurves of C-stars

J.M. Winters[1], A.J. Fleischer[1], A. Gauger[2], and E. Sedlmayr[1]

[1] Institut für Astronomie und Astrophysik, PN 8-1, Hardenbergstr. 36, 10623 Berlin, Federal Republic of Germany
[2] Los Alamos National Laboratory, Group T-4, MS B268, Los Alamos, NM 87545, USA

Received ; accepted

Abstract. Theoretical lightcurves of long–period and Mira variables are presented.

Based on dynamical models of circumstellar dust shells (CDS), which include time–dependent hydrodynamics and a detailed treatment of the processes of formation, growth and evaporation of carbon grains, frequency–dependent radiative transfer calculations have been carried out which yield the synthetic infrared lightcurves of these dust shell models.

It turns out that the discrete structure of the CDS due to the periodic formation of new dust layers decisively influences the shape of the lightcurves by producing e.g. intermediate extrema. This is demonstrated in detail for one model. Furthermore, dust shell models are presented whose lightcurves exhibit the superposition of two different oscillations: The oscillation with the period of the interior pulsation is superposed by an oscillation with a longer period which is produced by the dynamical structure of the CDS. Similar features are present in observed lightcurves, which indicates that our, nevertheless preliminary, modelling approach shows promise for interpreting the optical appearance of Miras and long–period variables.

Key words: hydrodynamics – radiative transfer – stars: carbon – circumstellar matter – stars: late–type

1. Introduction

Long–period variables (LPVs) are intrinsically cool objects many of which are surrounded by large amounts of dust. These dust particles are effective absorbers of radiative energy which they reradiate at longer wavelengths after an internal relaxation process (Woolf & Ney 1969; Gehrz & Woolf 1971). Therefore, most LPVs are primarily infrared sources.

Send offprint requests to: A.J. Fleischer

Improved instrumental capabilities in this spectral range and in the millimeter range have led to an increased interest in observations of late–type giants in the last years and produced a vast amount of observational data. This provided an extensive basis for a more thorough understanding of these objects. Based on this material e.g. Sopka et al. (1985), Claussen et al. (1987), Thronson et al. (1987), Willems & de Jong (1988), Jura et al. (1989), Jura & Kleinmann (1989), Groenewegen et al. (1992) were able to derive e.g. mass–loss rates, gas–to–dust ratios, distances, luminosities or final outflow velocities for various large samples of objects.

Compared to this kind of investigations relatively little attention was drawn to a systematic photometric monitoring of LPVs in the infrared range. The up–to–date most complete set of observations was published recently by Le Bertre (1992, 1993). His monitoring of C–stars (Le Bertre 1992) covered observations of 23 objects in the $1-20\mu$m range during a period of ≈ 6 years. He stresses the fact that the usage of parameters such as the phase at light maximum, the mean magnitude, and the peak–to–peak amplitude make sense only if the lightcurves were sinusoidal. However, the lightcurves of a large fraction of his sample of C–stars show “irregularities”, i.e. some lightcurves exhibit a plateau on their ascending branches or even intermediate extrema, especially at short wavelengths. Since these “irregularities” are reproducible from cycle to cycle, they have to be considered as real features of the lightcurves. In addition he notes that some lightcurves show a drift in time either of the average magnitude or of the amplitude. Similar behaviour with “bumps” and secondary maxima on the rising as well as on the declining branch is reported for visual lightcurves by Mattei et al. (1990).

Other authors, e.g. Lockwood & Wing (1971), Celis (1977), Werner et al. (1980), Feast et al. (1984), or Jones et al. (1990) presented photometric observations either for a more restricted time interval, for only one object or only at one wavelength, or with a less continuous coverage of the observed time interval.

Parallel to the advances on the observational part also the theoretical dynamical modelling of CDS around Miras and LPVs achieved fundamental improvements in the last years. Based on the pioneering papers of Willson & Hill (1979), Hill & Willson (1979), and Wood (1979), Bowen (1988) and Bowen & Willson (1991) improved this modelling approach by an inclusion of parameterized cooling laws which yield a more realistic modelling of the post–shock relaxation of the gas in the atmosphere. Very recently Feuchtinger et al. (1993) have formally overcome the problem of parameterized cooling laws by solving the complete set of equations of radiation hydrodynamics. Although their approach is physically consistent, i.e. they avoid the introduction of uncertain parameters by assuming LTE for describing the source function of the gas, a rigorous treatment of the relaxation processes would require a detailed non–LTE calculation.

All these models severely lack a detailed treatment of dust formation, growth and destruction, in particular Willson & Hill (1979) and Hill & Wilson (1979) did not include any dust at all. The other authors only use a simple formula, first introduced by Wood (1979) and later independently found by Bowen (1988), to simulate an additional acceleration due to radiation pressure on dust. This approach was insufficient to reveal the key role of the solid particles in determining the structure of the CDS (cf. Fleischer et al. 1991, 1992, henceforth called Paper I, and Fleischer 1994).

In Paper I we presented dynamical models of CDS around LPVs which include time–dependent hydrodynamics and a detailed treatment of the processes of formation, growth and evaporation of carbon grains. The models were calculated in the limit case of isothermal shocks (see Sect. 2.1). At least in the innermost, high–density region, where dust formation takes place, this approximation yields a realistic picture of the dynamical interactions which determine the global structure of the CDS and the effects discussed in the present paper. In the outer parts of the CDS the assumption of isothermal shocks might become invalid.

In the calculations of Paper I the radiative transfer problem is solved using the semi–analytical method of Lucy (1971, 1976) in grey approximation which yields a radiative equilibrium temperature structure at every instant of time but neither a spectrum nor a lightcurve of the model.

For the present investigation we have coupled the hydro–code of Paper I with the frequency–dependent radiative transfer code of Winters et al. (1994a) to study the optical appearance of our dust shell models.

We present theoretical lightcurves in the range of $0.5-25\mu$m for demonstrative model calculations of carbon–rich LPVs and draw a comparison to observed lightcurves.

We start with a short description of the modelling method in Sect. 2. In Sect. 2.1 we summarize our approach to calculate the dynamical structure of the shell. Section 2.2 comprises a brief description of the radiative transfer code and the coupling to the hydro–code. In Sect. 3 we present the results of our calculations. Since the details of the radial structure of the dust shell models have been discussed in Paper I, in Sect. 3.1 only the main features of these results are summarized. The lightcurves are presented in Sect. 3.2 and Sect. 3.3. As an example, we analyze in Sect. 3.2 for one typical model calculation in some detail how the shape of the lightcurve is influenced or even produced by the discrete structure of the CDS. In Sect. 3.3 we discuss the lightcurves of three different model calculations with respect to their long–term behaviour. The results are followed by a discussion in Section 4 where we compare our exemplary calculations with results from observations. We finish this paper with the conclusions in Sect. 5.

2. The modelling method

Since the details of the modelling method and the basic equations solved with both codes have been discussed elsewhere (Paper I, Winters et al. 1994a), here we only give a brief summary of the main ingredients.

2.1. Hydrodynamical model calculation

We consider a spherically symmetric shell around a pulsating red giant with mass $M_\star$, effective temperature $T_\star$, luminosity $L_\star$ and pulsation period P.

The time–dependent hydrodynamical equations are written in Lagrangian coordinates and solved by explicit integration according to the difference scheme given in Richtmyer & Morton (1967). Cooling of the gas behind the shock fronts is assumed to take place instantaneously, i.e. we treat the shocks in the isothermal limit case as in the calculations presented in Paper I. If cooling of the post–shock gas is taken into account, the interaction processes become even more complicated but the discrete structure of the CDS is conserved (Gauger et al. 1993a,b, 1994). However, since a main cause for the behaviour of the synthetic lightcurves (see Sect. 3) is the periodic formation of dust, we expect that the features presented here, will also appear in models where time–dependent post–shock cooling of the gas is taken into account.

The set of moment equations describing dust formation, growth and dust destruction due to thermal evaporation developed by Gail & Sedlmayr (1988) and Gauger et al. (1990) is solved simultaneously. For the calculation of the dust complex it is essential to know the chemical composition of the gas phase. We use the same set of hydrocarbons (H, H_2, C, C_2, C_2H, C_2H_2) in chemical equilibrium as in Paper I to calculate the particle densities of the species contributing to the growth of carbon grains. Solar abundances (Allen 1973) are assumed for all elements except for the abundance of carbon $\epsilon_{\rm C}$ which we consider as a free model parameter in order to account for a carbon–rich element composition.

For the calculation of the dynamical structure of the circumstellar shell the radiative transfer problem is treated by the semi–analytical method of Lucy (1971, 1976) which yields the local equilibrium temperature T_{eq} at every instant of time. Since we assume isothermal shocks the gas temperature T_g equals T_{eq} throughout the atmosphere at every instant of time.

At the inner boundary of the model a sinusoidal variation of the velocity with amplitude Δu and period P, the piston, is applied to simulate the interior pulsation of the star.

Thus, our models are defined by the prescription of the 4 fundamental stellar parameters ($T_\star$, $L_\star$, $M_\star$, $\epsilon_{\rm i}$) and of (P, Δu) to describe the interior pulsation. To start the calculation an initial hydrostatic model with the selected number of grid points (here 1024) and the desired values of $T_\star$, $L_\star$ and $M_\star$ is constructed. The velocity amplitude of the piston is increased slowly until the maximum value is reached and the calculation of the dust complex is started simultaneously. The development of the model is followed until a cyclic pattern of the radial structure is reached.

2.2. Radiative transfer calculation

For a given radial structure of the dust shell model, i.e. at a fixed instant of time, we solve the frequency–dependent stationary radiative transfer equation in spherical geometry. The radiation field is calculated by an iteration between the monochromatic moment equations (the system is closed by the variable Eddington factor) and the formal solution for the monochromatic specific intensity along the characteristic lines of the partial differential equation. At the inner boundary we apply the diffusion approximation in a form that provides a total flux of $L_\star/16\pi^2$ entering the atmosphere. The outer boundary condition is given by the assumption that no inward flowing radiation exists at $r = R_{\rm max}$. For details of this method we refer to Mihalas (1978).

The radiative transfer processes considered are grey absorption and thermal emission of the gas and frequency–dependent absorption and thermal emission of the dust component. In order to keep consistency with the hydrodynamical model, the transport coefficients of the gas are replaced by an average absorption coefficient $\kappa^{\rm g}$ which gives a gas opacity of $\kappa^{\rm g}/\rho = 2 \cdot 10^{-4}{\rm cm}^2{\rm g}^{-1}$ (ρ: mass density) (cf. Bowen 1988, Paper I). This value roughly represents the Rosseland mean gas opacity in the relevant temperature and density range.

For calculating the dust opacity the dust particles are assumed to be spherical and small compared to the relevant wavelength of the radiation field. The assumption of the *small particle limit* is approximately justified for the time–dependent models considered here, since the mean particle radius remains smaller than 0.1μm throughout the circumstellar shell (cf. Paper I). With these assumptions the absorption coefficient of the dust component $\kappa_\nu^{\rm d}$ can be expressed as (cf. Gail et al. 1984)

$$\kappa_\nu^{\rm d}(r) = \frac{8\pi^2 a_0^3}{\lambda} {\rm Im}\left\{\frac{m(\nu)^2-1}{m(\nu)^2+2}\right\} K_3(r) = \chi_\nu^{\rm d}(r)\,, \qquad (1)$$

and equals the extinction coefficient of the dust component $\chi_\nu^{\rm d}$. For all calculations presented here, the complex refractive index $m(\nu)$ of the grain material is taken from Maron (1990) which is appropriate for pure amorphous carbon grains. The quantity $K_3(r)$ is the third moment of the size distribution function $f(a,r)$ of the dust particles. It is defined by

$$a_0^3 K_3 = \int_{a_\ell}^\infty a^3 f(a,r) da\,, \qquad (2)$$

where a is the radius of the dust grain, a_0 denotes the hypothetical radius of a monomer contained in a dust grain, and a_ℓ is a lower limit size of the dust particles. Since we assume the dust particles to be small compared to the wavelength, we neglect the contribution of light scattering by the grains. Thus, the emissivity ϵ_ν is given by thermal emission of gas and dust:

$$\epsilon_\nu(r) = \epsilon_\nu^{\rm g}(r) + \epsilon_\nu^{\rm d}(r) = \kappa^{\rm g} B_\nu(T(r)) + \kappa_\nu^{\rm d} B_\nu(T(r))\,, \qquad (3)$$

where B_ν is the Kirchhoff–Planck function and the superscripts $^{\rm g}$ and $^{\rm d}$ denote the gas and the dust component, respectively.

By definition, K_3 equals the number of monomers condensed into grains per cm^3 and, therefore, is related to the degree of condensation f_c, i.e. the fraction of condensable material actually condensed into grains. In the case of pure carbon grains, which is considered here, the degree of condensation is given by

$$f_c = \frac{K_3}{(\epsilon_{\rm C} - \epsilon_{\rm O}) n_{<{\rm H}>}}\,, \qquad (4)$$

where we have assumed that all oxygen is locked up in the CO–molecule ($n_{<{\rm H}>}$: total density of hydrogen atoms). Thus, the radiative acceleration in units of the local gravitational deceleration

$$\alpha = \frac{\chi_H}{\rho} \frac{L_\star}{4\pi c G M_\star} \qquad (5)$$

is directly proportional to the degree of condensation in the small particle approximation (χ_H: flux–mean extinction coefficient, c: speed of light, G: gravitational constant).

Table 1. Parameters of the initial hydrostatic models. Also given are the time averaged mass loss rates and final outflow velocities of the evolved models.

	Model A*	Model B	Model C
$T_\star$ [K]	2600	2500	2450
ϵ_C/ϵ_O	1.8	1.34	1.25
$L_\star$ [$10^4\ L_\odot$]	1.0	1.0	3.0
$M_\star$ [$M_\odot$]	1.0	1.0	1.0
P [d]	650	370	621
Δu [km s^{-1}]	2.0	6.0	3.0
$< \dot{M} >$ [$M_\odot$ yr^{-1}]	1.0 10^{-5}	3.0 10^{-5}	2.9 10^{-4}
$< u_\infty >$ [km s^{-1}]	28.5	12.8	14.7

* Model A is equal to Model E of Paper I

3. Results

Table 1 shows the parameters of the initial hydrostatic models. Additionally given are the time averaged values of the mass loss rate and the final outflow velocity of the evolved models. Since there are few, if any, real objects for which all of these parameters are determined by observations, we have chosen the model parameters to represent prototypes of cool, dust–enshrouded carbon giants. For this kind of objects, e.g. Claussen et al. (1987) find typical values of the luminosity of the order of $10^4 L_\odot$, irrespective of the pulsational period. The investigations of Lambert et al. (1986) and Olofsson et al. (1993a,b) confirm, that the objects under consideration are in fact rather cool with effective temperatures well below or approximately 3000 K. Lambert et al. (1986) find e.g. for R Scl an overabundance of carbon to oxygen of 1.34 and an effective temperature of 2550 K. Olofsson et al. (1993a) quote a period of R Scl of 370 d, cf. Model B. IRC +10216, for instance, is known to be a highly evolved luminous source with a period exceeding 600 d, cf. Witteborn et al. (1980) and Ridgway & Keady (1988).

Since the model parameters inevitably had to be chosen following different observational investigations, one cannot expect that the sets of parameters satisfy the various fit–formulae obtained from the results of certain evolutionary calculations (e.g. core mass–luminosity relations (cf. Boothroyd & Sackmann 1988), or the radius–mass–luminosity relation (Iben 1984)). Furthermore, our sets of model parameters do not fit to the well known period–mass–radius relations of Ostlie & Cox (1986), which were derived from linear, nonadiabatic pulsation analysis calculations for oxygen–rich, less luminous ($L_\star \leq 7000\ L_\odot$) models with stellar temperatures between 2700 K and 3400 K.

In contrast to other authors (e.g. Bowen (1988) and Bowen & Willson (1991)) who rely on these formulae, we have chosen to stay with the *observationally* derived quantities for this study.

3.1. Radial structure of the dust shell models

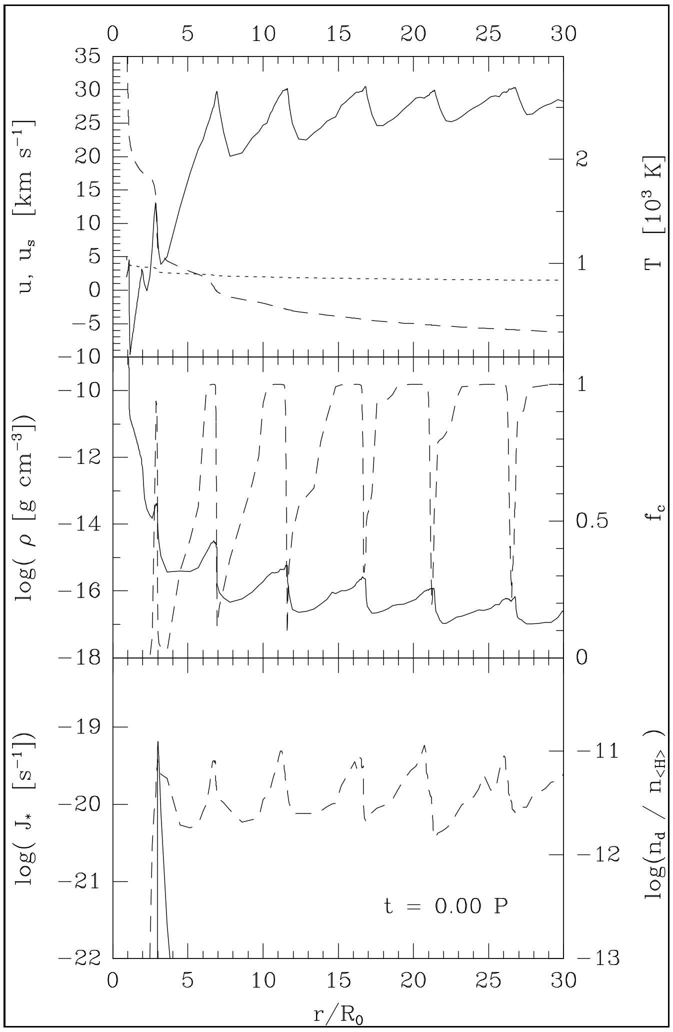

Fig. 1. Radial structure of Model A at $t = 0.00P$.

Figure 1 depicts a typical radial structure of the CDS at the beginning of the hydrodynamical cycle shown for Model A, cf. Table 1. The following quantities are plotted:

upper diagram: the velocity u (solid line), velocity of sound u_s (dotted line) and the temperature T (dashed line),

middle diagram: the logarithm of the density ρ (solid line) and the degree of condensation f_c, i.e. the fraction

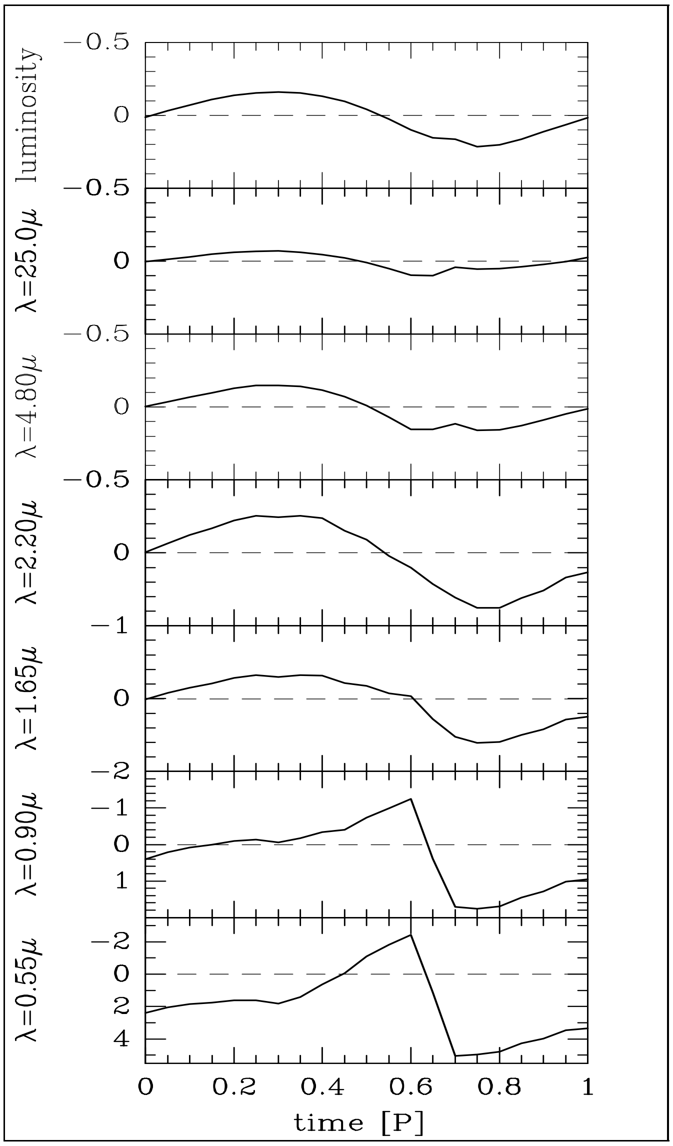

Fig. 2. Theoretical lightcurves (in magnitudes, relative to the mean magnitude) of Model A at different wavelengths over a time interval of one pulsational period. Note the different scaling of the ordinate at different wavelengths.

of condensable material actually condensed into grains (dashed line) (cf. Eq. (4)),

lower diagram: the logarithm of the nucleation rate $J_\star$, i.e. the number of dust grains formed per second and H–atom (solid line) and the logarithm of the number of dust grains per H–atom $n_{\rm d}/n_{<\rm H>}$ (dashed line).

Radii are always given in units of the stellar radius R_0 of the initial hydrostatic model.

The consistent calculation of dust formation and grain growth and destruction shows up to have significant influence on the resulting dynamical structure of the CDS. As the degree of condensation and the number of dust grains per H–atom in Fig. 1 show, the dust is distributed inhomogeneously across the shell. The dust grains are concentrated in distinct layers, equidistant for each model, and exhibit a shell or onion like structure which is closely related to the hydrodynamical structure of the CDS.

Fig. 1 also shows the determining influence of the dust on the thermodynamical structure of the CDS. There are several steps in the course of the temperature which coincide with spikes in the degree of condensation.

These interactions are investigated in detail in Paper I and, therefore, are only briefly summarized here.

The discrete structure of the atmosphere is not produced solely by the shock waves caused by the interior pulsation of the star, but is a very product of the process of dust formation. In a first step the interior pulsation defines the onset of dust *formation* by providing appropriate low temperatures in the region between 3 and $4R_0$. In a second step pulsation triggers grain *growth* by a compression of the material in this radius interval and, thus, provides densities favourable for the growth process. In a short time interval values of f_c as high as 1 are reached, i.e. all condensable material is actually condensed into grains. The quantity f_c is proportional to the radiative acceleration of the dust grains (cf. Paper I and Eqs. (1), (4), (5)). Since the grains are closely momentum coupled to the gas, the sudden increase of the radiative acceleration causes a perturbation in the velocity field which steepens to become a shock wave, thereby compresses the material and, in turn, accelerates dust growth. Thus, the prominent shock waves which propagate through the atmosphere (cf. Fig. 1) are produced by a self–accelerating mechanism caused by dust formation.

Furthermore, the newly formed dust in the inner shells, due to its opacity, effectively blocks the outgoing radiation and heats the material closer to the star. This back–warming, seen as steps in the temperature structure in Fig. 1, also influences the formation of new dust particles.

Due to pulsation and back–warming, dust formation and growth is only possible in a small radius range and during a limited time interval. This results in the discrete structure of the CDS. The complex interplay among the processes of dust formation and growth, hydrodynamics and thermodynamics shows that the dust particles play the key role in determining the atmospheric structure of LPVs and Miras. The influence of periodic dust formation on the lightcurves of these objects is discussed in detail for Model A in the next section.

3.2. The lightcurves of Model A, detailed analysis

The theoretical lightcurves of Model A are displayed in Fig. 2 for several wavelengths between 0.55μm and 25μm during a time interval of one hydrodynamical period P. The sinusoidal variation of the inner boundary (cf. Sect. 2.1) is reflected by the temporal variation of the stellar luminosity, shown in the upper panel of Fig. 2. Apart from the smooth temporal variation of the flux which is

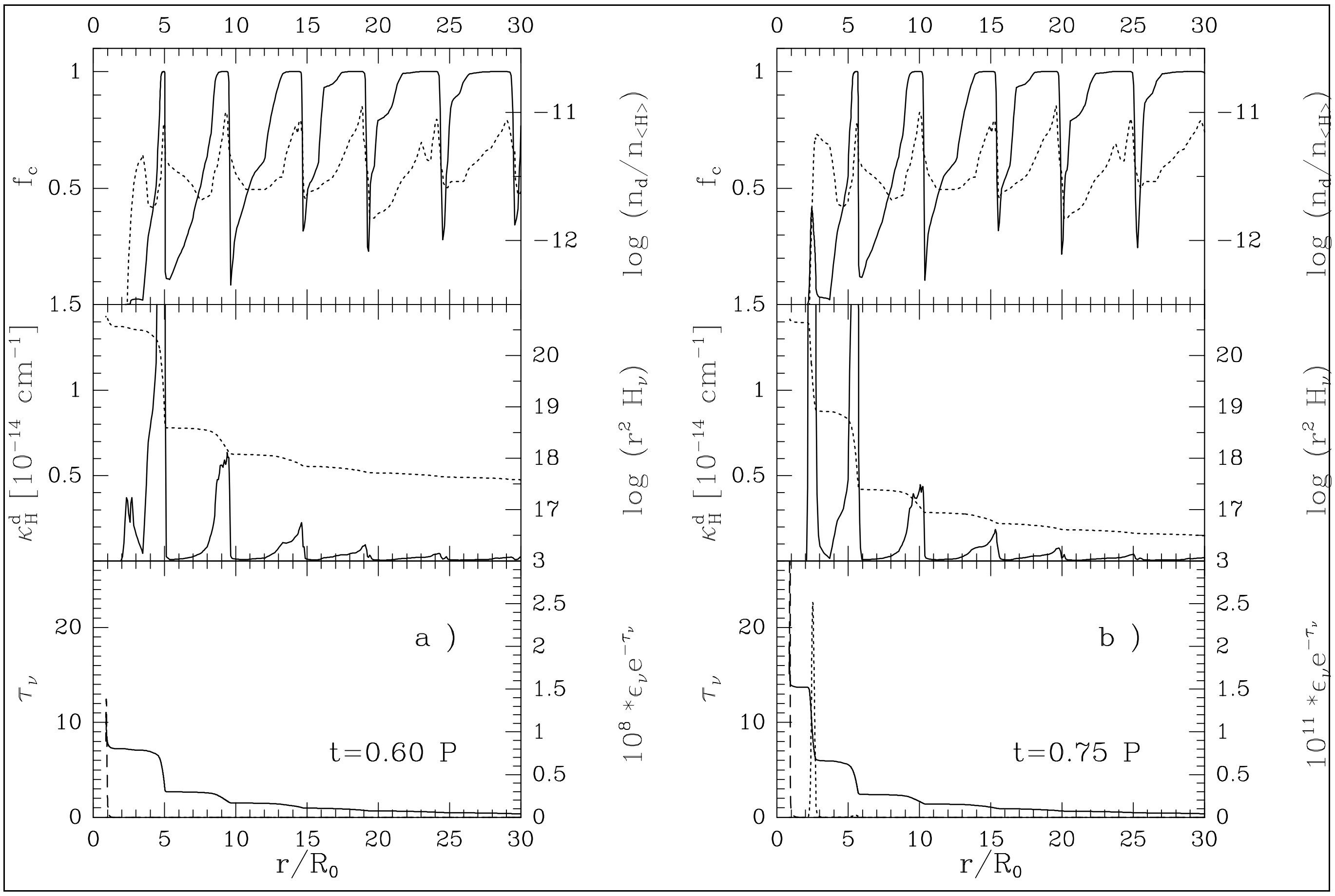

Fig. 3. Radial structure of Model A at **a)** the beginning of the dust formation cycle at $t = 0.60P$ and **b)** at $t = 0.75P$. The quantities shown are explained in the text. $r^2 H_\nu$ is given in [erg s^{-1}Hz^{-1}] and $\epsilon_\nu e^{-\tau_\nu}$ in [erg s^{-1}cm^{-3}sr^{-1}Hz^{-1}]. Frequency–dependent quantities refer to a corresponding wavelength of $\lambda = 0.90\mu$m.

caused by this luminosity variation, the long wavelength lightcurves ($\lambda > 2.2\mu$m) additionally exhibit pronounced narrow secondary maxima which occur periodically within the third quarter of the pulsational cycle (cf. Fig. 5). In the short wavelength lightcurves ($\lambda < 2.2\mu$m), the variation due to the luminosity is almost completely concealed by strong features occuring periodically around $t = 0.60P$. The maximum value of these peaks decreases towards longer wavelengths until the pronounced structure eventually disappears at $\lambda = 2.2\mu$m. The flux minimum seen at $t = 0.70$P in the short wavelength lightcurves exactly corresponds to the intermediate maximum in the long wavelength lightcurves.

The occurrence of these striking features in the lightcurves is an immediate consequence of the dynamical behaviour of the discrete dust layers.

In Figs. 3 and 4 the radial course of several quantities which are of interest for the following discussion of the lightcurves are shown at four selected instants during the pulsational cycle. The quantities shown in these figures are:

upper diagram: the degree of condensation f_c (solid line) and the logarithm of the particle density of dust grains $n_{\rm d}$ normalized to the total hydrogen particle density $n_{<{\rm H}>}$ (dashed line),

middle diagram: the flux mean absorption coefficient of the dust component κ_H^d (solid line) and the logarithm of the Eddington flux H_ν at $\lambda = 0.90\mu$m passing through the spherical surface at radius r, multiplied by r^2 to eliminate the pure geometrical dilution (dashed line),

lower diagram: the total (gas and dust) optical depth τ_ν at $\lambda = 0.90\mu$m (solid line), the local contribution of dust emission to the 0.90μm *intensity* reaching the outer shell boundary in radial direction $\epsilon_\nu^d e^{-\tau_\nu}$ (short–dashed line) and the respective contribution due to gas emission $\epsilon_\nu^g e^{-\tau_\nu}$ (long–dashed line).

We start the discussion of the lightcurves at time $t = 0.60P$ shortly after the beginning of a new dust formation cycle (cf. Fig. 3a)). At this instant, all dust layers present in the circumstellar shell are fully developed, i.e. the degree of condensation within these layers

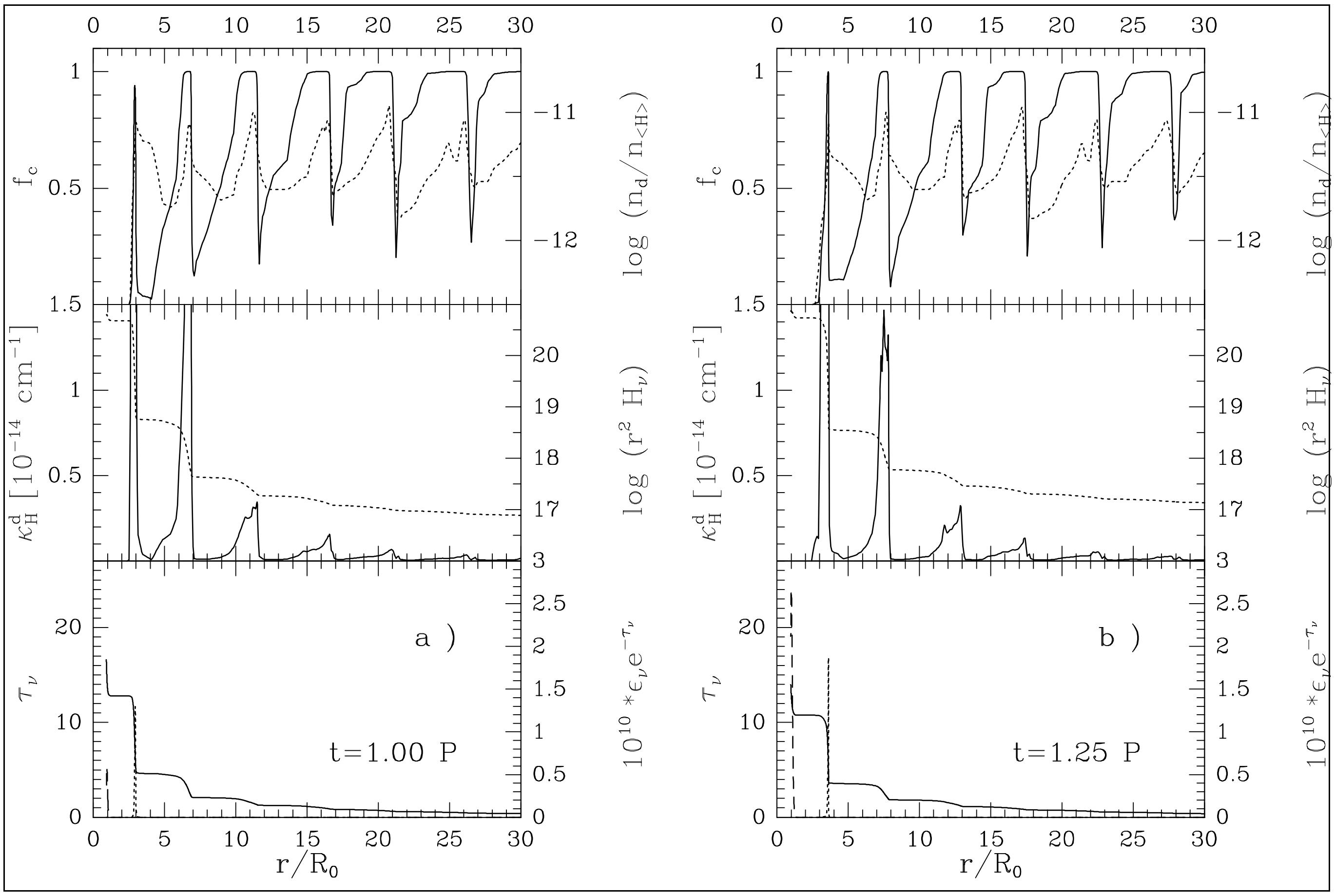

Fig. 4. Same as Fig. 3 at **a)** $t = 1.00P$ and **b)** at $t = 1.25P$, again at $\lambda = 0.90\mu$m.

has reached its maximum value of 1 and the layers are moving outwards. At $t = 0.60P$ the total dust optical depth has reached its minimum value during the cycle, the dust optical depth at $\lambda = 0.90\mu m$ is $\tau_{0.90\mu} = 7.23$. Simultaneously the short wavelength lightcurves reach their peak value (cf. Fig. 2). Due to the relatively small optical depth, the dominant contribution to the short wavelength radiation that escapes from the shell is produced by photospheric gas emission (cf. Fig. 3a)). Between $t = 0.60P$ and $t = 0.70P$ a new dust layer begins to form as indicated by the enhanced particle density of dust grains already at $t = 0.60P$ seen in Fig. 3a) around $3R_0$. At this instant new dust particles condense from the gas phase, but these particles are still too small to produce a relevant degree of condensation. Although the nuclei already show up in the flux mean absorption coefficient $\kappa_H^{\rm d}$, they still do not influence the optical depth at this time. The newly formed dust particles subsequently grow very effectively and, thereby, increase the optical depth of the new dust layer. From $t = 0.70P$ on, the short wavelength photospheric radiation is already effectively blocked by the new layer (cf. the radial variation of the Eddington flux in Figs. 3a) and b)). At the same time the minimum value of the short wavelength lightcurves is reached, whereas in the long wavelength lightcurves a shallow intermediate maximum occurs. The main contribution to the short wavelength flux is now provided by thermal dust emission, originating from the front of the innermost dust shell (note the different scaling of the source contribution $\epsilon_\nu e^{-\tau_\nu}$ in Figs. 3a) and b). Note also that the *flux* is given by an angle integration of $\epsilon_\nu e^{-\tau_\nu}$ and, thus, the respective source contribution is weighted by the radiating surface). At longer wavelengths, absorption of the stellar radiation field is less effective, and thermal dust emission from the newly formed layer contributes a significant fraction to the emergent flux and produces the retarded intermediate structure in the long wavelength lightcurves. At $t = 0.75P$ the degree of condensation in the newly formed dust layer has reached a value of $f_c = 0.41$ (cf. Fig. 3b)), the optical depth of the new layer alone has increased to $\Delta\tau_{0.90\mu} = 7.75$ and, thus, produces the innermost step of the τ–structure displayed in Fig. 3b) (the optical depth of the new layer at 25μm is $\Delta\tau_{25\mu} = 0.21$ at this instant). During the following time interval until $t = 1.00P$ the optical depth of the new dust layer increases up to its maximum value of $\Delta\tau_{0.90\mu} = 8.40$ due to growth of the dust grains, whereas the degree of condensation reaches the maximum possible value of $f_c = 1$ not until $t = 1.25P$ (cf. the sequence of Figs. 3b), 4a), b)). Obviously, there are two competing processes during this phase: Between $t = 0.75P$ and $t = 1.00P$ dust formation and growth exceeds the dilution of the material due to expansion, whereas between $t = 1.00P$ and $t = 1.25P$ expansion predominates. Simultaneously, the outer layers merely expand and due to geometrical dilution of the material the optical depth in front of the newly formed layer decreases. Within this time interval the short wavelength radiation which escapes from the dust envelope is predominantly produced by thermal emission of dust located in the outer part of the new layer. This changes at $t = 1.35P$, when the total optical depth has reached a value of $\tau_{0.90\mu} = 9.70$. Due to expansion, caused by radiation pressure on the new dust shell, the innermost layer has become increasingly transparent ($\Delta\tau_{0.90\mu} = 6.50$ at $t = 1.35P$) and cooler. At this time the contribution of photospheric gas emission again exceeds the contribution emerging from the radiating dust layer. Simultaneously, the short wavelength lightcurves start to rise steeply until $t = 1.60P$, when the total optical depth of the shell has again reached its minimum value of $\tau_{0.90\mu} \approx 7$, with the innermost dust layer contributing $\Delta\tau_{0.90\mu} = 4.37$ to this value.

Thus, in the case of Model A discussed here, we can clearly distinguish two different phases within one hydrodynamical period which are essentially characterized i) by effective dust formation and growth (between $t = 0.60P$ and $t \approx 1.00P$) and ii) by expansion of the dust layers (between $t \approx 1.20P$ and $t = 1.60P$). During the relatively short first part of phase i), where very effective dust formation and growth takes place, the optical depth of the circumstellar shell increases from almost zero at $t = 0.60P$ to $\Delta\tau_{0.90\mu} = 7.75$ at $t = 0.75P$ and, thus, leads to the steep decline of the short wavelength lightcurves. Due to expansion of the dust layers during phase ii), the optical depth decreases, which results in the increase of the short wavelength lightcurves. In the long wavelength lightcurves the formation of a new dust layer between $t = 0.60P$ and $t = 0.75P$ leads to the intermediate maxima seen in Figs. 2 and 5, which are caused by thermal dust emission originating from the new layer.

A necessary condition for the strong features in the lightcurves to occur, produced by the mechanism of dust formation, is the existence of distinct phases, during which the respective competing processes (dust formation and expansion) are subject to very different time scales. For Model A this is the case in the interval between $t = 0.60P$ and $t = 0.75P$ where the time scale of grain growth τ_{gr} is considerably shorter than the expansion time scale τ_{exp} and between $t = 1.25P$ and $t = 1.60P$, where expansion predominates due to radiative acceleration of the new layer. For Models B and C these distinct phases are multiple times longer, cf. the discussion in the next section.

Summarizing the preceding discussion, we state:

- The occurrence of the intermediate structures in the lightcurves critically depends on the temporal evolution of the optical depth of the innermost dust layer.
- The short wavelength radiation seen during the peak of the lightcurves of Model A (between $t = 0.35P$ and $t = 0.70P$, cf. Fig. 2) is mainly produced by photospheric gas emission.

3.3. The lightcurves of Models A – C, long-term analysis

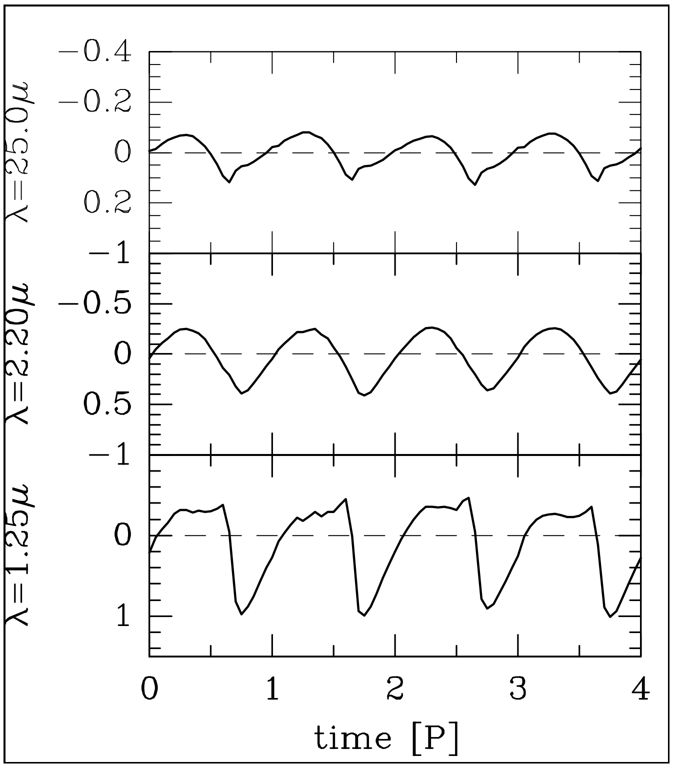

Fig. 5. Theoretical lightcurves (in magnitudes, relative to the mean magnitude) of Model A at different wavelengths. Note the different scaling of the ordinate at different wavelengths.

Figs. 5, 6 and 7 show the lightcurves of Models A – C for three representative wavelengths.

Fig. 5 shows the long–term behaviour of the lightcurves of Model A which has been discussed in detail in the previous section. From the periodic occurrence of the intermediate structures at $\lambda = 1.25\mu$m and $\lambda = 25\mu$m it can be inferred that the formation of a new dust layer periodically takes place during every second half of the hydrodynamical cycle. The lightcurve at 25μm shows a slightly asymmetric shape and exhibits an internal structure on the rising branch which regularly occurs and is even more pronounced at longer wavelengths.

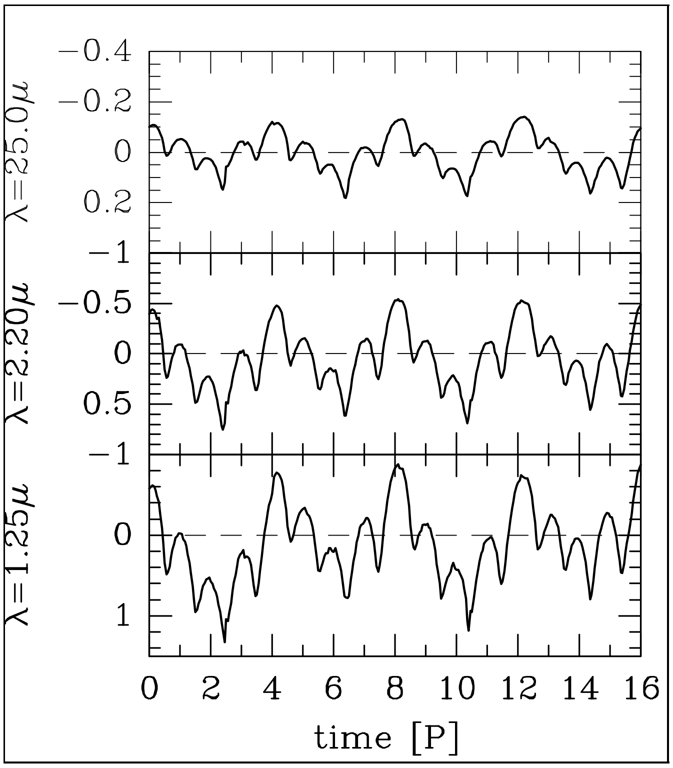

Fig. 6. Theoretical lightcurves (in magnitudes, relative to the mean magnitude) of Model B at different wavelengths. Note the different scaling of the ordinate at different wavelengths.

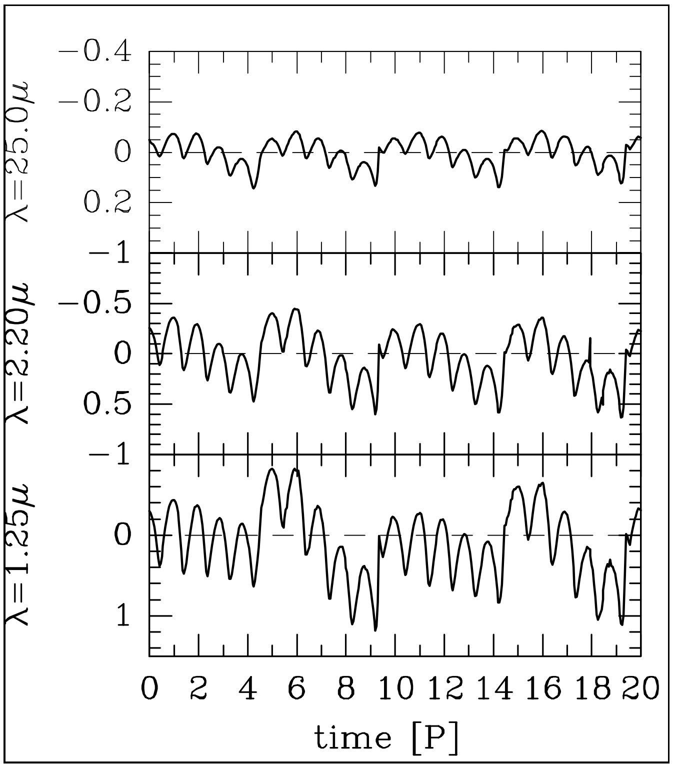

Fig. 7. Theoretical lightcurves (in magnitudes, relative to the mean magnitude) of Model C at different wavelengths. Note the different scaling of the ordinate at different wavelengths.

All curves are characterized by a periodic re–occurrence of all features at the same phase during the sequence of hydrodynamical pulsation cycles.

In contrast to Model A, Models B and C exhibit a different behaviour. These models (cf. Fig. 6 and 7) show alternating high maxima at all wavelengths. Models B and C show a quasi–sinusodial behaviour on the scale of one pulsational period which is superposed by a long–scale oscillation. To get an idea how these surprising finding could be explained we have to go back to the results of the hydrodynamical calculations.

In Paper I it was mentioned that, depending on the carbon abundance $\epsilon_{\rm C}$, the formation of a new dust shell can take place *every* hydrodynamical period, as is the case for Model A, but also every second, third ...pulsational period, i.e. the radial structure of the CDS at a certain instant of time $t = \beta P$ equals the structure at $t = (\beta + n_P)P$, where β is an arbitrary dimensionless time parameter and $n_P = 1, 2, \ldots$ is the *multiperiodicity* number. A detailed analysis of the occurrence of multiperiodicity is beyond the scope of the present paper. We just state that for Model B $n_P = 4$, for Model C $n_P = 5$ whereas for Model A $n_P = 1$. In principle, the process of the formation of a new dust shell is the same in Models B and C as described in detail for Model A. The difference is the timescale: The formation of a fully evolved new dust layer takes a time interval of four pulsational cycles in Model B compared to one pulsational cycle for Model A.

Obviously, the course of the lightcurves at longer wavelengths, e.g. at 25.0μm reflects the global dynamical behaviour of the dust shell model. A new dust layer is formed at each of the deep minima at $t \approx 2.5, 6.5, 10.5 \ldots$ P, respectively (cf. Fig. 6). The newly formed layers move outwards and reach their maximum degree of condensation just before the next layer is formed, i.e. at $t \approx 6.0, 10.0, 14.0 \ldots$ P, respectively.

The minima at $t \approx 2.5, 6.5, 10.5 \ldots$ P (cf. Fig. 6) have an alternating depth at shorter wavelengths. This is due to a slight variation of approximately 0.5 R_0 of the exact radial location where the new dust layer is formed. Caused by the local hydrodynamical conditions at $t \approx 2.5, 10.5, \ldots$ P dust formation already starts at slightly smaller radii and, therefore at higher densities which leads to a larger optical depth of the newly formed layer. Thus, the course of the short wavelength lightcurves sensitively probes the physical conditions in the innermost region of the dust shell.

Model C behaves similar to Model B, therefore a detailed description is omitted here.

A detailed analysis of the effect of *multiperiodicity* will be the subject of a forthcoming paper (Fleischer et al. 1994).

4. Discussion

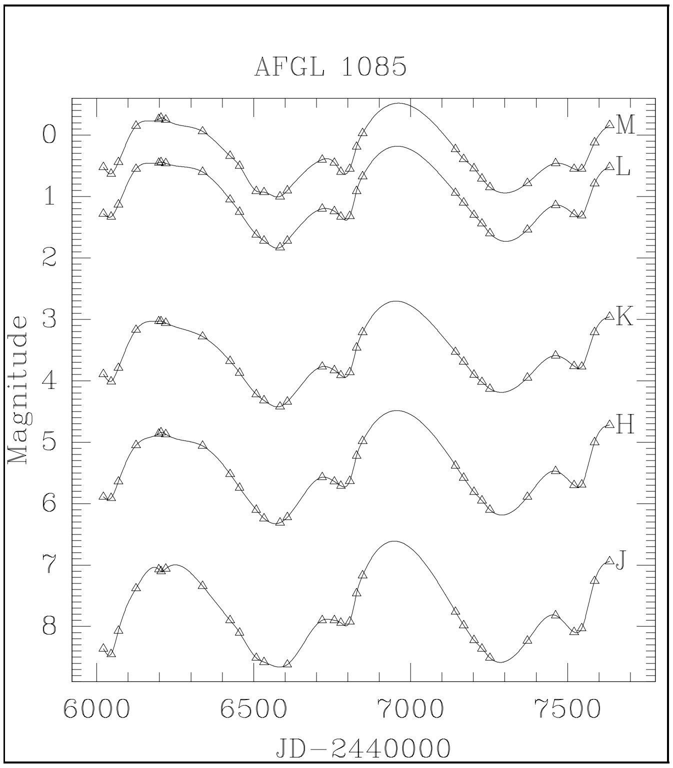

Fig. 8. Observed lightcurves of AFGL 1085, data are taken from Le Bertre (1992)

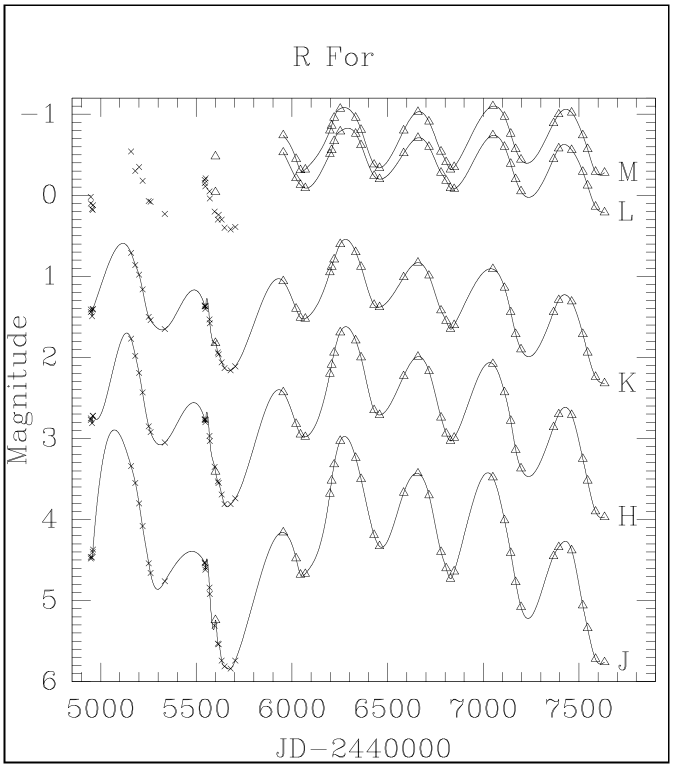

Fig. 9. Observed lightcurves of R For, data are taken from (△): Le Bertre (1992) and (×): Feast et al. (1984)

We do not intend to model a special object but to present results of a theoretical investigation, which is devoted to the principle physical mechanisms, and reveals an important influence of the dynamical structure on the optical appearance of LPVs and Miras. Thus, we cannot expect a quantitative agreement between our model calculations and the observations but at most a qualitative agreement of certain characteristic features.

To draw this comparison we choose the measured lightcurves of two objects of the sample of Le Bertre (1992), AFGL 1085 and the carbon–rich Mira R Fornacis (cf. Figs. 8, 9). For R For it is possible to combine the data of Le Bertre with those of Feast et al. (1984), except for a slight disagreement of the L photometric fluxes. Therefore, we omitted these data when we connected the measured points of R For and AFGL 1085 by a cubic spline interpolation (the M fluxes were not measured by Feast et al. 1984).

The characteristic features of the AFGL 1085 lightcurves (cf. Fig. 8) are the intermediate extrema, already noted by Le Bertre (1992). With respect to our model calculations, these intermediate structures could be caused by the sudden formation of a new dust layer similar to Model A.

In the short wavelength lightcurves ($\lambda < 2.2\mu$m) of Model A the dynamical behaviour of the discrete dust layers causes rather narrow, additional maxima, which are steeply decreasing in time due to the rapid increase of the dust optical depth. These additional maxima follow the broad, plateau–like maxima produced by the varying luminosity (cf. Figs. 2 and 5). At longer wavelengths ($\lambda > 2.2\mu$m), on the other hand, the periodic formation of new dust layers leads to shallow intermediate maxima on the ascending branches of the lightcurves, which are produced by thermal dust emission originating mainly from these new layers. Due to the wavelength dependence of the dust opacity, the features in the synthetic lightcurves, which are produced by absorption of photospheric radiation at shorter wavelengths and by dust emission at longer wavelengths, accordingly depend on the wavelength.

However, the intermediate structures present in the observed lightcurves (e.g. AFGL 1085) could also be caused by different mechanisms, e.g. by the dissipation of shock wave energy in the inner parts of the atmosphere (cf. Feuchtinger et al. 1993) which is transferred to the radiation field. Furthermore, the formation of secondary shocks in the innermost dust–free region (the occurrence of which has thoroughly been investigated by Bowen 1990 and Willson et al. 1994) could also lead to such intermediate structures in the lightcurves. In both cases, the *strength* of the secondary maxima might also depend on the wavelength, but we do not expect that these mechanisms could produce minima at shorter wavelengths and simultaneously maxima at longer wavelengths. To decide, whether dust formation is responsible for the occurrence of the observed intermediate maxima, the promising objects (e.g. AFGL 1085, R Lep, …(see Le Bertre 1992)) should be simultaneously monitored with a sufficient temporal resolution during the phases of interest in a wide spectral regime (e.g. between 0.90μm and 100μm).

The presence of discrete dust layers in our models also causes rippled or even step–like structures in the radial brightness profiles as well as in the theoretical visibilities, which result from these calculations (cf. Winters 1994). Similar structures have been observed e.g. for IRC +10216 (Ridgway & Keady 1988). A detailed discussion of these results will be subject to a forthcoming paper (Winters et al. 1994b).

Since the discrete structure of the dust shell may provide an explanation for both, the occurrence of intermediate structures in the lightcurves as well as the pronounced structures in observed brightness distributions, from a theoretical point of view, we would favour the dust mechanism described in the present paper to be responsible for the bumps in the lightcurves.

The lightcurves of R For (cf. Fig. 9) show a systematic drift in magnitude very similar to the multiperiodic Model B. Feast et al. (1984) found R For to exhibit an "anomaleously" deep minimum in 1983. A similar deep minimum has been observed in 1990 by Le Bertre (1992). Secondary variations with characteristic time scales multiple times longer than the main period have also been found in the lightcurves of several other objects by Alksnis (1990).

In terms of our model calculations we could explain this behaviour by the interplay of two distinct processes with different time scales: The regular pulsation of the star, which provides the "short" hydrodynamical time scale, and the process of dust formation and growth, which, under the conditions of Models B and C has a time scale of four respectively five times longer. Thus, the CDS can be conceived as a dynamical system under the influence of an external exciting mechanism, or, to use a simple analogy from classical mechanics, the CDS behaves similar to a pendulum, which is subject to a periodic external force.

We expect from our model calculations that observations of R For continuing the monitoring of Le Bertre (1992) would again reveal a long–term increase of the lightcurves.

5. Conclusions

Theoretical lightcurves of carbon–rich long–period and Mira variables are presented.

Based on dynamical models of CDS, which include time–dependent hydrodynamics and a detailed treatment of the processes of formation, growth and evaporation of carbon grains (cf. Paper I), frequency–dependent radiative transfer calculations have been carried out which yield the synthetic lightcurves of these dust shell models.

It is demonstrated how the complex interplay among the processes of dust formation and growth, hydrodynamics and thermodynamics decisively influences the short–scale behaviour as well as the long–term course of the lightcurves. The dust component plays the key role in producing features, such as intermediate extrema and secondary periods, which similarly occur in observed lightcurves.

The comparison between our theoretical lightcurves and the observations shows that our simple coupling of the dynamical dust shell calculations and the radiative transfer calculations is a promising approach to understand the optical appearance of LPVs and Miras. Thus, although the models presented here are still preliminary, theoretical modelling has been improved by the consistent inclusion of the dust formation process and we have found new phenomena in these models that show promise to explain some observed phenomena that have until now been puzzling. On the observational part a simultaneous monitoring of LPVs and Miras in a wide spectral region with an appropriate temporal resolution is desirable to improve the observational data base and to allow a detailed comparison with improved theoretical model calculations in the near future.

Acknowledgements. We are grateful to the referee L.A. Willson for helpful suggestions, especially for bringing to our attention the fact that Bowen (1988) and Wood (1979) independently came up with the same simple formula for approximating the radiation pressure on dust. We thank W. Rauter for collecting the observational data from the literature and preparing Figs. 8 and 9. The calculations were performed on the CRAY computers of the Konrad–Zuse–Zentrum für Informationstechnik Berlin and the HLRZ, Jülich. Subsequent data analysis has been performed on the WAP–cluster of the physics department of the TU Berlin. This work has been partly supported by the Deutsche Forschungsgemeinschaft, *DFG*–Schwerpunkt "Theorie kosmischer Plasmen" (grant Se 420/5–4).

References

Alksnis A., 1990, Variability of Carbon Stars. In: Mennessier M.O., Omont A. (eds.) From Miras to Planetary Nebulae: Which Path for Stellar Evolution. Editions Frontières, Gif sur Yvette Cedex, p. 279

Allen C.W., 1973, Astrophysical Quantities, The Athlone Press, London

Boothroyd A.I., Sackmann I.-J., 1988, ApJ 328, 641

Bowen G.H., 1988, ApJ 329, 299

Bowen G.H., 1990, Dynamical phenomena in pulsating star atmospheres. In: Buchler J. R. (ed.) The numerical modelling of nonlinear stellar pulsations. NATO ASI Series C, Kluwer Academic Publishers, p. 155

Bowen G.H., Willson L.A., 1991, ApJ 375, L53

Celis L., 1977, A&AS 29, 15

Claussen M.J., Kleinmann S.G., Joyce R.R., Jura, M., 1987, ApJS 65, 385
Feast M.W., Whitelock P.A., Catchpole R.M., Roberts G., Overbeek M.D, 1984, MNRAS 211, 331
Feuchtinger M.U., Dorfi E.A., Höfner S., 1993, A&A 273, 513
Fleischer A.J., 1994, Dissertation, TU Berlin
Fleischer A.J., Gauger A., Sedlmayr E., 1991, A&A 242, L1
Fleischer A.J., Gauger A., Sedlmayr E., 1992, A&A 266, 321 (Paper I)
Fleischer A.J., Gauger A., Sedlmayr E., 1994, A&A in preparation
Gail H.-P., Keller R., Sedlmayr E., 1984, A&A 133, 320
Gail H.-P., Sedlmayr E., 1988, A&A 206, 153
Gauger A., Gail H.-P., Sedlmayr E., 1990, A&A 235, 345
Gauger A., Fleischer A.J., Winters J.M., Sedlmayr E., 1993a, AG Abstr. Series 9, 127
Gauger A., Fleischer A.J., Winters J.M., Sedlmayr E., 1993b, Circumstellar shells of long–period variables: Dust formation and optical appearance. In: Clegg R., Meikle P., Stevens I. (eds.) Circumstellar Media in the late stages of stellar evolution. Cambridge Univ. Press, in press
Gauger A., Fleischer A.J., Sedlmayr E., 1994, A&A in preparation
Gehrz R.D., Woolf N.J., 1971, ApJ 165, 285
Groenewegen M.A.T., de Jong T., van der Bliek N.S., Slijkhuis S., Willems F.J., 1992, A&A 253, 150
Hill S.J., Willson L.A., 1979, ApJ 229, 1029
Iben I. Jr., 1984, ApJ 277, 333
Jones T.J., Bryja C.O., Gehrz R.D., et al., 1990, ApJS 74, 785
Jura M., Joyce R.R., Kleinmann S.G., 1989, ApJ 336, 924
Jura M., Kleinmann S.G., 1989, ApJ 341, 359
Lambert D.L., Gustafsson B., Eriksson K., Hinkle K.H., 1986, ApJS 62, 373
Le Bertre T., 1992, A&AS 94, 377
Le Bertre T., 1993, A&AS 97, 729
Lockwood G.W., Wing R.F., 1971, ApJ 169, 63
Lucy L.B., 1971, ApJ 163, 95
Lucy L.B., 1976, ApJ 205, 482
Maron N., 1990, Ap&SS 172, 21
Mattei J.A., Cannizzo J.K., Goodings D.A., 1990, AAVSO data files on pulsating stars and chaos studies on three long period variables. In: Cacciari C., Clementini G. (eds.) Confrontation between stellar pulsation and evolution. ASP Conf. Ser. Vol. 11, p.461
Mihalas D., 1978, Stellar Atmospheres. 2nd. ed., W.H. Freeman & Co., San Francisco
Olofsson H., Eriksson K., Gustafsson B., Carlström U., 1993a, ApJS 87, 267
Olofsson H., Eriksson K., Gustafsson B., Carlström U., 1993b, ApJS 87, 305
Ostlie D.A., Cox A.N., 1986, ApJ 311, 864
Richtmyer R.D., Morton K.W., 1967, Difference methods for initial–value problems, 2^{nd} ed., John Wiley & Sons, New York
Ridgway S.T., Keady J.J., 1988, ApJ 326, 843
Sopka R.J., Hildebrand R., Jaffe D.T., et al., 1985, ApJ 294, 242
Thronson H.A., Latter W.B., Black J.H., Bally J., Hacking P., 1987, ApJ 322, 770
Werner M.W., Beckwith S., Gatley I., Sellgren K., Berriman G., 1980, ApJ 239, 540
Willems F.J, de Jong T., 1988, A&A 196, 173
Willson L.A., Hill S.J., 1979, ApJ 228, 854
Willson L.A., Struck–Marcell C., Bowen G.H., 1994, Winds from pulsating stars. In Jokipii J.R., Sonett C.P., and Giampapa M.S. (eds.), Cosmic Winds and the Heliosphere, University of Arizona Press, Tucson, in press
Winters J.M., 1994, Dissertation, TU Berlin
Winters J.M., Dominik C., Sedlmayr E., 1994a, A&A in press
Winters J.M., Fleischer A.J., Gauger A., Sedlmayr E., 1994b, A&A in preparation
Witteborn F.C., Strecker D.W., Erickson E.F., et al., 1980, ApJ 238, 577
Wood P.R., 1979, ApJ 227, 220
Woolf N.J., Ney E.P., 1969, ApJ 155, L181

This article was processed by the author using Springer-Verlag LaTeX A&A style file *L-AA* version 3.